



Contents lists available at ScienceDirect



# Catalysis Today

journal homepage: [www.elsevier.com/locate/cattod](http://www.elsevier.com/locate/cattod)

## Heteropolyacid catalysts for Diels-Alder cycloaddition of 2,5-dimethylfuran and ethylene to renewable *p*-xylene

Yanuar Philip Wijaya<sup>a,1</sup>, Haryo Pandu Winoto<sup>a,b,1</sup>, Young-Kwon Park<sup>c</sup>, Dong Jin Suh<sup>a,d</sup>, Hyunjoo Lee<sup>a,b</sup>, Jeong-Myeong Ha<sup>a,b,e</sup>, Jungho Jae<sup>a,b,\*</sup>

<sup>a</sup> Clean Energy Research Center, Korea Institute of Science and Technology, Seoul 02792, Republic of Korea

<sup>b</sup> Clean Energy and Chemical Engineering, Korea University of Science and Technology, Daejeon 34113, Republic of Korea

<sup>c</sup> School of Environmental Engineering, University of Seoul, Seoul 02504, Republic of Korea

<sup>d</sup> Department of Green Process and System Engineering, Korea University of Science and Technology, Daejeon 34113, Republic of Korea

<sup>e</sup> Green School, Korea University, Seoul 02841, Republic of Korea

### ARTICLE INFO

#### Article history:

Received 19 August 2016

Received in revised form

19 November 2016

Accepted 16 December 2016

Available online xxx

#### Keywords:

Biomass

Diels-Alder

2,5-Dimethylfuran

*p*-Xylene

Heteropolyacids

### ABSTRACT

The Diels-Alder cycloaddition of biomass-derived furans and subsequent dehydration are promising routes for the sustainable production of commodity chemicals such as *p*-xylene (PX). In this paper, we have investigated the catalytic performances of a range of phosphotungstic acid (HPW) and silicotungstic acid (HSiW) catalysts supported on various oxides, i.e., SiO<sub>2</sub>, Al<sub>2</sub>O<sub>3</sub>, TiO<sub>2</sub> and ZrO<sub>2</sub> and their structure-activity correlation in the conversion of 2,5-dimethylfuran (DMF) and ethylene to PX. The characterization studies of the catalysts using XRD, BET, Raman and <sup>31</sup>P MAS-NMR spectroscopy reveal that all of the supported heteropolyacid (HPA) catalysts (except HPW/ZrO<sub>2</sub>) retain their Keggin structure on the surface of oxide supports. Results from ammonia- and *n*-propylamine-TPD studies show that all of the supported HPA catalysts possess well-defined Brønsted acid sites with the total acidity decreasing in the following order: HPA/SiO<sub>2</sub> > HPA/Al<sub>2</sub>O<sub>3</sub> > HPA/ZrO<sub>2</sub> > HPA/TiO<sub>2</sub>. The conversion of DMF and the initial rate of PX production generally increase with an increase in the total acidity, with HPA/SiO<sub>2</sub> being the most active catalyst. The turnover frequency of PX production for HPA/SiO<sub>2</sub> is also considerably greater than those for the HPAs supported on Al<sub>2</sub>O<sub>3</sub>, ZrO<sub>2</sub>, and TiO<sub>2</sub>, which suggests that the higher activity of HPA/SiO<sub>2</sub> is at least partly due to the enhanced strength of Brønsted acid sites. Both the silica-supported HSiW and HPW catalysts demonstrate remarkably high PX selectivity (82–85%) at high DMF conversion (91–94%) at 250 °C after 6 h reaction. The effects of reaction conditions such as acid loading, reaction temperature, and reaction time have also been investigated with the most active silica-supported HSiW catalysts to optimize the PX yield.

© 2016 Elsevier B.V. All rights reserved.

## 1. Introduction

The potential of utilizing biomass as a renewable resource to reduce the dependency on petroleum-based resources has driven research efforts towards the development of sustainable processes for the production of aromatic chemicals, such as benzene, toluene, and xylenes (BTX) [1–3]. The sustainability of BTX aromatics is critical because they are used widely in fuels and in the chemicals industry as the precursors for polymers [3]. In particular, *p*-xylene (PX) is a precursor chemical for the synthesis of

polyethylene terephthalate (PET), a thermoplastic polymer with applications in fibers, packaging, and electric devices manufacture [4–6]. Fig. 1 presents a fully sustainable integrated process for the production of PX from biomass (the major steps are marked with the bold arrow lines). Glucose, as the major product from the hydrolysis of cellulose, can be isomerized to fructose using biological (i.e. enzymes) [7] or thermochemical catalysts such as Sn-containing beta zeolite [8]. Fructose can then be dehydrated to 5-hydroxymethylfurfural (HMF), which is subsequently converted to 2,5-dimethylfuran (DMF) via hydrogenolysis [9,10]. Meanwhile, glucose can also be fermented to produce ethanol [11], which is then dehydrated to ethylene [12,13]. The reaction between DMF and ethylene can then occur via tandem Diels-Alder cycloaddition (DA) and dehydration reactions to produce PX.

\* Corresponding author at: Clean Energy Research Center, Korea Institute of Science and Technology, Seoul 02792, Republic of Korea.

E-mail addresses: [jjae@kist.re.kr](mailto:jjae@kist.re.kr), [john.jjae@gmail.com](mailto:john.jjae@gmail.com) (J. Jae).

<sup>1</sup> Co-first authors.

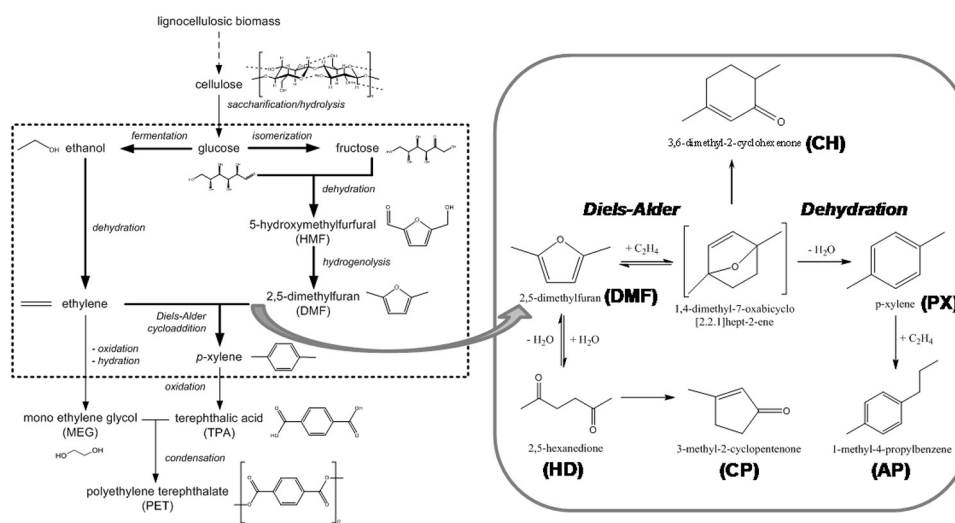


**Fig. 1.** A sustainable process for conversion of biomass to renewable p-xylene (PX), a precursor chemical for synthesis of polyethylene terephthalate (PET) and the reaction network for PX production from DMF and ethylene via a DA-dehydration cascade.

In the recent years, intensive research has been done over a range of acid catalysts [14–21] because a promising route for the production of renewable PX from DMF was introduced over the H-Y zeolite with good selectivity (~75%). It was reported that the overall rate of PX formation is controlled by the initial DA reaction step over H-Y because Brønsted acids cannot catalyze the DA reaction [14]. A DFT study also revealed the rate-limiting step to be the DA reaction when Brønsted acids are used and dehydration when Lewis acids such as Na-Y are used [15]. In a different study, acidic oxides (such as  $\text{WO}_x\text{-ZrO}_2$  and niobic acid) were reported to have superior activity for the production of aromatics (~77% PX selectivity) and higher resistance to coke deposition than zeolite Y due to its strong Brønsted acidity [16]. More recently, higher PX selectivity (90%) at almost complete (~99%) DMF conversion was achieved over H-BEA zeolite ( $\text{Si}/\text{Al} = 12.5$ ) in *n*-heptane for 24 h reaction [17]. On the other hand, another research group reported that microporous materials, such as H-BEA zeolite, are less resistant to coke deposition than mesoporous materials [16,20]. Its microporosity is the cause of the mass-transfer limitation to the catalytic active sites due to the significant pore resistance, leading to catalyst deactivation [20] and the requirement of frequent regeneration in a continuous process [16]. As an alternative, a mesoporous beta zeolite with a morphology similar to a nanospunge (NSP-BEA) was introduced as a highly active and stable catalyst (~80% PX selectivity, ~99% DMF conversion, at 24 h reaction with 50 bar ethylene pressure) [20]. The advantage of using a mesoporous catalyst was also reported, in which approximately 70% PX selectivity at 90% DMF conversion was achieved over silica-alumina aerogel (SAA) with well-defined large mesopores of 20–30 nm at a shorter reaction time (6 h) [18]. All previous reports revealed the good catalytic performances of solid acid catalysts with strong Brønsted acid sites for PX production from DMF via DA and dehydration reactions; however, most of the reactions for producing high PX yield (>80%) were carried out for a long time (>24 h). A long-time reaction could be tedious, impractical, and economically unattractive. Herein, we propose another potential catalyst for achieving a comparably high PX yield and remarkable PX selectivity within a shorter reaction time.

Heteropolyacids (HPAs) with a Keggin structure, such as phosphotungstic acid ( $\text{H}_3\text{PW}_{12}\text{O}_{40}$ ) and silicotungstic acid ( $\text{H}_4\text{SiW}_{12}\text{O}_{40}$ ), have received a lot of interest as promising acid catalysts for a range of chemical reactions owing to their purely strong Brønsted acidity [22–27]. Solid HPAs possess stronger acidity and a unique structure that differs from ordinary mineral

acids and solid acid catalysts, such as zeolites and metal oxides [22,24,25,28]. Keggin-type HPAs have a discrete ionic structure that consists of heteropolyanions with the formula  $[\text{XW}_{12}\text{O}_{40}]^{n-}$  ( $\text{X} = \text{P}^{5+}, \text{Si}^{4+}, \text{Al}^{3+}, \text{Co}^{2+}$ , etc.) and counterions ( $\text{H}^+$ ,  $\text{H}_3\text{O}^+$ ,  $\text{H}_5\text{O}_2^+$ , etc.), which stabilize the Keggin units [22,28–31]. This network structure enables the protons to be very active and extremely mobile, not only on the surface, but also within the interior of the solid HPA crystallites [22,23,29]. In addition, the Keggin-structure HPAs are more thermally stable with a simpler synthesis procedure than the HPAs of other structures [24,27]. The supported HPA has been reported to exhibit higher catalytic activity than silica-alumina, oxides, and acidic zeolites for relatively low temperature reactions [23,29,30], such as the synthesis of dimethyl ether (DME) via dehydration of methanol over oxide-supported HPA [29,30]. Overall, HPAs are regarded as economically and environmentally attractive catalysts that can be used widely in both homogeneous and heterogeneous reactions [22,32].

In this study, we have investigated the catalytic performances of a range of phosphotungstic acid (HPW) and silicotungstic acid (HSiW) catalysts supported on various oxides, i.e.,  $\text{SiO}_2$ ,  $\text{Al}_2\text{O}_3$ ,  $\text{TiO}_2$  and  $\text{ZrO}_2$  and their structure–activity correlation in the conversion of DMF and ethylene to PX. Their catalytic performances were also compared with those of H-Beta zeolites (H-BEA,  $\text{Si}/\text{Al} = 12.5$  and 19) and silica-alumina aerogel (SAA,  $\text{Si}/\text{Al} = 1$ ), which were previously reported as highly active catalysts. The activity correlation of HPAs supported on different oxides was explored based on the acid site density and acid strength. The effects of reaction conditions, such as acid loading, reaction temperature, and reaction time, were also investigated with the most active silica-supported HSiW catalyst. Importantly, this study demonstrated the superior catalytic performance of silica-supported HSiW towards the presently most active commercial catalyst for PX production, H-BEA ( $\text{Si}/\text{Al} = 12.5$ ).

## 2. Experimental

### 2.1. Catalyst preparation

All of the supported HPA catalysts were prepared by the incipient wetness method with an ethanol solution at room temperature, as described elsewhere [29]. Bulk phosphotungstic acid (HPW, Aldrich, >99.9%) and silicotungstic acid (HSiW, Aldrich, >99.9%) were used as the reference materials and dried overnight at 100 °C. The incipient wetness volume of the ethanol solution was esti-

mated based on the ratio of HPA to the oxide supports (10–20 wt%). After impregnation, the samples were kept at room temperature for 24 h to reach a uniform distribution of HPA clusters onto the oxide supports, and then dried in an oven at 100 °C for 24 h. The silica-, alumina-, titania-, and zirconia-supported HPW and HSiW are referred to as HPW/SiO<sub>2</sub> and HSiW/SiO<sub>2</sub>, HPW/Al<sub>2</sub>O<sub>3</sub> and HSiW/Al<sub>2</sub>O<sub>3</sub>, HPW/TiO<sub>2</sub> and HSiW/TiO<sub>2</sub>, and HPW/ZrO<sub>2</sub> and HSiW/ZrO<sub>2</sub>, respectively. SiO<sub>2</sub> was used as received for impregnation, whereas Al<sub>2</sub>O<sub>3</sub>, TiO<sub>2</sub>, and ZrO<sub>2</sub> were calcined at 400 °C in air for 5 h before impregnation.

H-BEA-25 (CP814E, Si/Al atomic ratio = 12.5), H-BEA-38 (CP814C, Si/Al atomic ratio = 19), and H-ZSM-5 (CBV3024E, Si/Al atomic ratio = 15) were purchased from Zeolyst. Silica-alumina aerogel (SAA) with Si/Al atomic ratio = 1 (SAA-57) was prepared using the method described elsewhere [18]. The zeolites and SAA were calcined at 550 °C in air for 4 h before reaction.

## 2.2. Characterization

Powder X-ray diffraction (XRD, Shimadzu LabX-XRD 6000) measurements were performed using Cu K $\alpha$  radiation ( $\lambda = 1.54 \text{ \AA}$ ) from 5 to 50° 2θ. The Brunauer-Emmett-Teller (BET) surface areas and porosity of catalysts were determined by recording the N<sub>2</sub> adsorption-desorption isotherms using a BELSORP-mini II apparatus (BEL Japan, Inc.). Before analysis, the samples of bulk HPW and HSiW were outgassed at 150 °C for 3 h, whereas the samples of the supported catalysts were outgassed at 200 °C for 3 h. The Raman spectra of bulk and supported HSiW catalysts were recorded in a Jobin Yvon T64000 with a visible laser (532 nm) excitation. The <sup>31</sup>P MAS NMR spectra of bulk and supported HPW catalysts were recorded in a Bruker Avance 400 WB spectrometer at a frequency of 8 kHz. The acid properties of the bulk and supported HPA catalysts were determined by ammonia-temperature programmed desorption (NH<sub>3</sub>-TPD) measurements using a BELCAT-B catalyst analyzer coupled with a thermal conductivity detector (TCD) and a mass spectrometer (MS). TPD was performed over the temperature range, 100–850 °C, after the saturation of catalyst surface with NH<sub>3</sub> at 100 °C for 25 min. TPD of *n*-propylamine (Sigma Aldrich, >99%) was also carried out to confirm the formation of Brønsted acid sites on the supported HPA catalysts. Samples (50 mg) were impregnated with 0.25 cc of propylamine and vacuum dried at 40 °C prior to analysis. Subsequently, the TPD measurements were performed over the temperature range, 100–750 °C, with gas detection through a MS.

## 2.3. Catalytic experiments

The reactions were performed in a 160 mL high pressure Parr reactor. A mixture of DMF (3.9 mL) and 1,4-dioxane (30 mL) and each HPA catalyst (0.05–0.15 g) were charged into the reactor at first. After sealing the reactor, the reactor was purged three times with N<sub>2</sub>. The reactor was then pressurized with ethylene to 20–30 bar and heated to 225–300 °C. The reaction mixture was stirred at 350 rpm with an impeller and the reactions were performed for 1–10 h. At the end of the reaction, the reactor was cooled by air cooling fan and the liquid content was sampled and analyzed by GC-FID (Agilent 7890A) and GC-MS (Agilent 5975). The quantification of products was undertaken by creating calibration curves for each product compound using standard chemicals.

## 3. Results and discussion

### 3.1. Characterization of bulk and supported HPA catalysts

The structural, surface and acid properties of the bulk and supported HPA catalysts were investigated by XRD, N<sub>2</sub> physisorp-

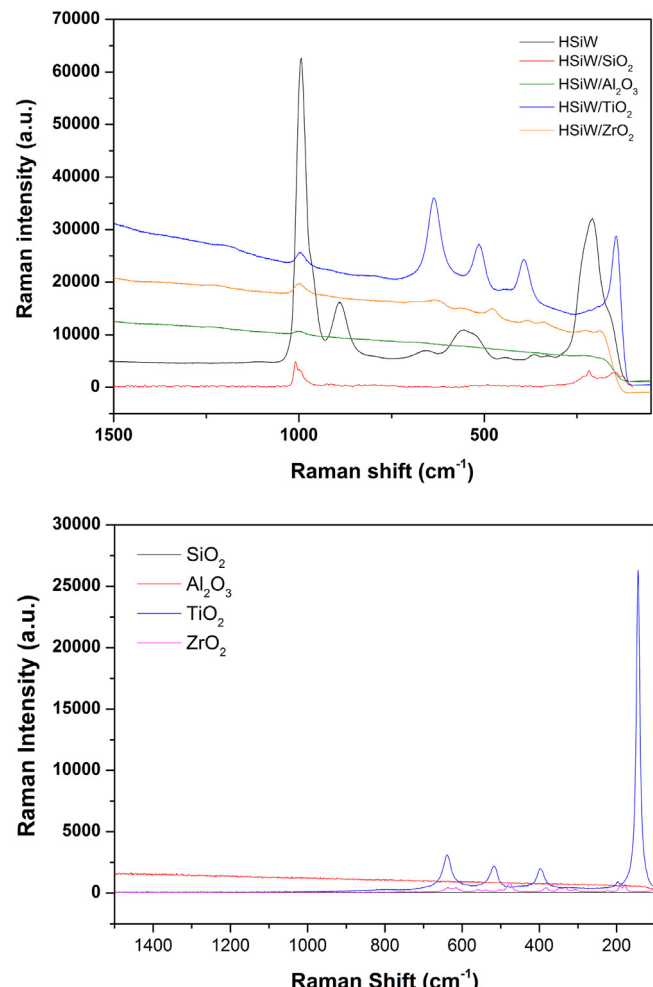


**Fig. 2.** Raman spectra for bulk and supported HSiW catalysts (top) and support materials (bottom).

tion, Raman spectroscopy, <sup>31</sup>P MAS NMR, and ammonia- and propylamine-TPD analyses. The XRD patterns of the bulk HPW and HSiW showed intensive reflections at 10.3°, 25.3°, and 34.8° 2θ, belonging to the typical Keggin structure of HPAs (see Fig. S1) [33,34]. These XRD peaks were not observed for Al<sub>2</sub>O<sub>3</sub>, TiO<sub>2</sub>, and ZrO<sub>2</sub> supported HPAs, indicating that HPW and HSiW are highly dispersed on the supports. Meanwhile, the XRD patterns of HPAs supported on SiO<sub>2</sub> exhibited definite peaks at 10.3°, 25.3°, and 34.8° 2θ. This suggests that heteropolyanions tend to agglomerate into larger clusters on the silica support, forming X-ray detectable crystallites. Fig. 2 shows the Raman spectra of bulk and supported HSiW catalysts. The spectrum of bulk HSiW exhibited intense bands at 998, 974, 882, 555, and 227 cm<sup>-1</sup>, which were assigned to the symmetric and asymmetric stretching modes of  $\nu(W=O)$ , asymmetric stretching mode of  $\nu(W-O-W)$ , and the bending modes of  $\nu(O-Si-O)$  and  $\nu(W-O-W)$  [34,35]. All the oxide-supported HSiW catalysts showed a Raman band at 998 cm<sup>-1</sup> for the W=O stretching band, indicating that the Keggin structure of HSiW was well preserved on the surface of the oxide supports. However, the band intensity at 998 cm<sup>-1</sup> was varied with support used and HSiW/Al<sub>2</sub>O<sub>3</sub> exhibited a relatively weaker intensity of the band as compared to those of other supported HSiW, implying that less W=O bonds are present on HSiW/Al<sub>2</sub>O<sub>3</sub>. In addition to the Raman peak at 998 cm<sup>-1</sup>, HSiW/TiO<sub>2</sub> showed strong bands at 144, 399, 519, and 639 cm<sup>-1</sup>, which were related to the Raman bands of the TiO<sub>2</sub> nanoparticles.

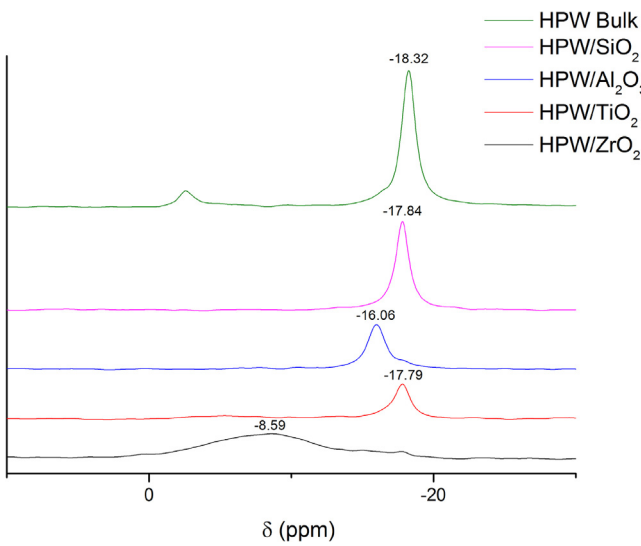


**Fig. 3.**  $^{31}\text{P}$  NMR spectra of bulk and supported HPW catalysts.

**Fig. 3** shows the  $^{31}\text{P}$  MAS NMR spectra of bulk and supported HPW catalysts. Hydrated HPA species of the Keggin structure give a strong resonance in the range of  $-15$  to  $-18$  ppm, depending on their hydration degree [36]. HPW supported on  $\text{SiO}_2$ ,  $\text{Al}_2\text{O}_3$ , and  $\text{TiO}_2$  exhibited a peak at  $-17.8$ ,  $-16.0$  and  $-17.8$  ppm, respectively, indicating that the Keggin structure of HPW remains intact on these supports. Meanwhile, HPW/ $\text{ZrO}_2$  showed a broad peak at  $-8.6$  ppm, which can be assigned to lacunary species formed by partial decomposition of HPW on  $\text{ZrO}_2$ , with a shoulder peak at  $-17.8$  ppm [36,37]. This result indicates that a great amount of HPW on  $\text{ZrO}_2$  stays as fragment forms of HPW. It was reported

that zirconia disrupts the Keggin structure of HPAs owing to its basic properties, resulting in strong interaction between HPA and zirconia surface [31].

**Table 1** lists the textural properties (BET surface area and total pore volume) of the HPAs supported on different oxides. The BET surface areas and total pore volumes of the neat supports decreased in the order:  $\text{SiO}_2 > \text{Al}_2\text{O}_3 > \text{ZrO}_2 > \text{TiO}_2$ . In general, the addition of HPW and HSiW to the supports resulted in a slight decrease in surface area, except for  $\text{Al}_2\text{O}_3$ . In the case of  $\text{Al}_2\text{O}_3$ , it is possible that HPA molecules are mostly located outside the pore, which leads to an increase in the surface area of the alumina-supported HPAs. The surface areas and pore volumes of the HPAs supported on the oxides decreased in the same order as the neat supports. Assuming a Keggin unit cross section of  $144\text{ \AA}^2$  for HPA molecules [30], 15% HPA loading will correspond to a monolayer HPA coverage of  $45\text{ m}^2\text{ g}^{-1}$ . Because all of the oxide supports used in this study had surface areas above  $45\text{ m}^2\text{ g}^{-1}$ , it is expected that all the supported HPA catalysts would have submonolayer HPA coverage.

The acidic properties of the bulk and supported HPA catalysts were investigated using  $\text{NH}_3$ -TPD. **Fig. 4** shows the  $\text{NH}_3$ -TPD curves for the neat supports and HPA catalysts, and **Table 1** lists the total acidity. The bulk HPW and HSiW exhibited three  $\text{NH}_3$  desorption peaks at  $100\text{--}200^\circ\text{C}$  (denoted as  $\alpha$ -peak),  $200\text{--}450^\circ\text{C}$  (denoted as  $\beta$ -peak), and  $450\text{--}600^\circ\text{C}$  (denoted as  $\gamma$ -peak). The  $\alpha$ -peak was assigned to the desorption of hydrogen-bonded  $\text{NH}_3$  molecules, while the  $\beta$ - and  $\gamma$ -peaks were attributed to the decomposition of ionically bonded  $\text{NH}_4^+$  ion coordinated in the different crystal lattices [25]. Regarding the neat supports,  $\text{Al}_2\text{O}_3$ ,  $\text{TiO}_2$ , and  $\text{ZrO}_2$  showed two  $\text{NH}_3$  desorption peaks at temperatures of  $150$  and  $430^\circ\text{C}$ ,  $150$  and  $270^\circ\text{C}$ , and  $150$  and  $430^\circ\text{C}$ , respectively, whereas  $\text{SiO}_2$  showed only a weak and broad peak at  $400^\circ\text{C}$ . In terms of the total acidity, the  $\text{Al}_2\text{O}_3$  support showed the highest total acidity ( $0.31\text{ mmol/g}$ ) followed by  $\text{TiO}_2$  ( $0.28\text{ mmol/g}$ ),

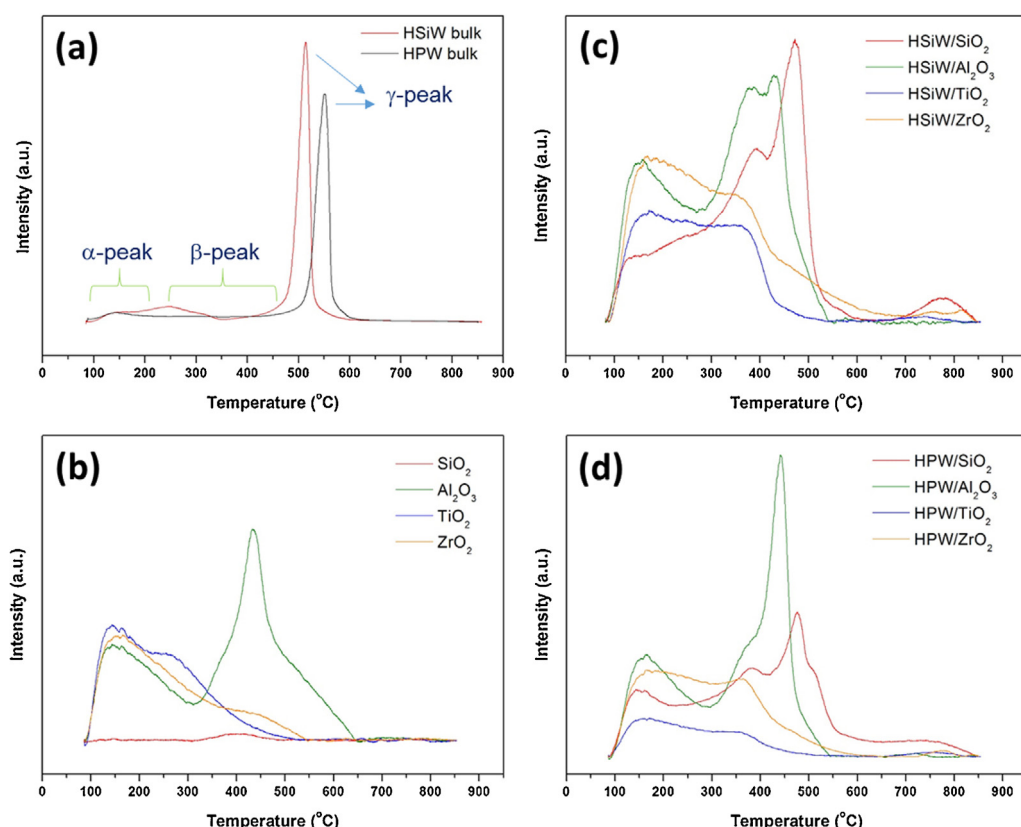


**Fig. 4.**  $\text{NH}_3$ -TPD profiles of Keggin HPA catalysts: bulk HSiW and HPW (a), metal oxide supports (b), oxide-supported HSiW (c), and oxide-supported HPW (d).

**Table 1**

Summary of textural and acid properties of catalysts used in this study.

Entry	Catalyst	Si/Al	$S_{BET}^a$ ( $m^2/g$ )	$V_{pore}^b$ ( $cm^3/g$ )	$D_{pore}^c$ (nm)	$C_{acid}^d$ (mmol/g)
1	SiO <sub>2</sub>	n.a.	176	1.48	58.1	0.02
2	Al <sub>2</sub> O <sub>3</sub>	n.a.	87	1.03	21.3	0.31
3	TiO <sub>2</sub>	n.a.	58	0.69	43.6	0.28
4	ZrO <sub>2</sub>	n.a.	89	0.41	7.1	0.17
5	HPW	n.a.	6.6	0.22	37.4	2.03
6	15%-HPW/SiO <sub>2</sub>	n.a.	150	1.62	37.4	1.05
7	15%-HPW/Al <sub>2</sub> O <sub>3</sub>	n.a.	92	1.01	43.6	0.82
8	15%-HPW/TiO <sub>2</sub>	n.a.	48	0.73	76.5	0.36
9	15%-HPW/ZrO <sub>2</sub>	n.a.	77	0.34	6.3	0.50
10	HSiW	n.a.	5.8	0.19	37.4	2.30
11	15%-HSiW/SiO <sub>2</sub>	n.a.	152	2.28	43.6	1.14
12	15%-HSiW/Al <sub>2</sub> O <sub>3</sub>	n.a.	103	1.01	21.3	1.04
13	15%-HSiW/TiO <sub>2</sub>	n.a.	51	0.66	23.6	0.40
14	15%-HSiW/ZrO <sub>2</sub>	n.a.	82	0.41	6.3	0.54
15	H-BEA-25	12.5	545	0.49	9.4	1.12 <sup>[18]</sup>
16	SAA-57	1	411	1.39	28.1	1.16 <sup>[18]</sup>
17	H-BEA-38	19	475	0.34	3.8	1.21 <sup>[18]</sup>
18	H-ZSM-5	15	358	0.23	2.4	1.10 <sup>[18]</sup>

Notation: <sup>a</sup>BET surface area, <sup>b</sup>Single point total pore volume ( $P/P_0 = 0.98$ ), <sup>c</sup>Average pore diameter obtained by BJH method, <sup>d</sup>NH<sub>3</sub>-TPD total acid site; n.a. = not applicable.

ZrO<sub>2</sub> (0.17 mmol/g), and SiO<sub>2</sub> (0.02 mmol/g). In general, supported HPA catalysts showed higher total acidity than their parent supports, indicating that the impregnation of HPA into the supports induced new acid sites. In particular, HPW (1.05 mmol/g) and HSiW (1.14 mmol/g) supported on SiO<sub>2</sub> showed much higher total acidity compared to SiO<sub>2</sub> (0.02 mmol/g). The NH<sub>3</sub>-TPD profiles of HPW/SiO<sub>2</sub> and HSiW/SiO<sub>2</sub> showed three NH<sub>3</sub> desorption peaks appearing at 150, 390, and 475 °C and at 130, 400, and 475 °C, respectively, which should be due to the interaction of NH<sub>3</sub> molecules with HPA. In the case of HPAs supported on Al<sub>2</sub>O<sub>3</sub>, TiO<sub>2</sub> and ZrO<sub>2</sub>, an additional NH<sub>3</sub> desorption peak appeared at 350–380 °C, compared to their parent supports. The total acidity of HPW and HSiW supported on SiO<sub>2</sub>, Al<sub>2</sub>O<sub>3</sub>, TiO<sub>2</sub>, and ZrO<sub>2</sub> decreased in the order: SiO<sub>2</sub> > Al<sub>2</sub>O<sub>3</sub> > ZrO<sub>2</sub> > TiO<sub>2</sub>. It appears that the weak interaction of silica with the HPAs keeps their Brønsted acid character and results in an increase in total acidity.

TPD of *n*-propylamine was also performed to confirm the formation of Brønsted acid sites on the supported HPA catalysts. Because propylamine decomposes to propene and ammonia only at the Brønsted acid sites, the number of molecules that decompose can be indicative of the Brønsted acidity [38]. It was found that propylamine decomposed completely to ammonia and propene over all of the supported HSiW catalysts at 350–380 °C (see Fig. S2). Therefore, it is believed that the supported HSiW catalysts used in this study possess predominantly Brønsted acid sites.

### 3.2. Catalytic performances of bulk and supported HPA catalysts

At the initial stages, the catalytic performances of the bulk and supported HPA catalysts were investigated in a short reaction time (1 h) and compared with the previously tested catalysts, such as H-BEA-25, H-BEA-38, H-ZSM-5, and SAA-57. As shown in Fig. 5 and Table 2, bulk HPW and HSiW were quite active for the conversion of DMF (41–71%) and selective toward the PX production (46–53% selectivity), demonstrating their effectiveness for catalyzing the DA reaction of DMF and ethylene. Regarding the oxide-supported HPAs, their activity and selectivity to PX was strongly dependent on the type of support. For both HPW and HSiW, the conversion of DMF and the selectivity to PX decreased in the following order: HPA/SiO<sub>2</sub> > HPA/Al<sub>2</sub>O<sub>3</sub> > HPA/TiO<sub>2</sub> > HPA/ZrO<sub>2</sub>. The PX production rate also decreased in the same order, indicating that silica better promotes the activity of HPAs, followed in order by alumina, titania, and zirconia, possibly due to its higher surface area, larger pore volume, and higher acidity (see the comparison in Table 1). Among the supported HPAs, the silica-supported HSiW exhibited

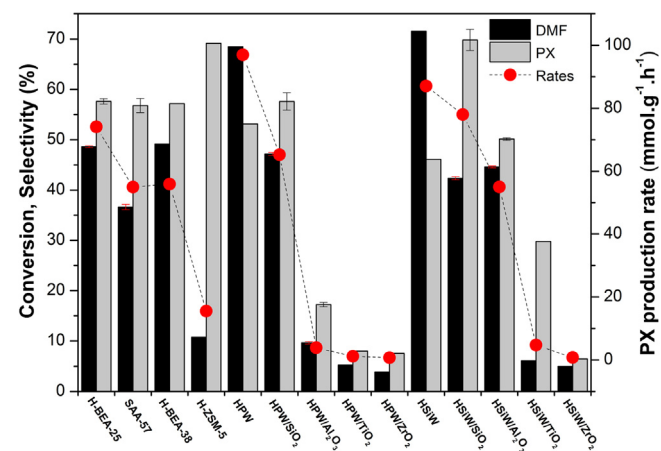


**Fig. 5.** DMF conversion, PX selectivity, and PX production rate for the DA-reaction of DMF and C<sub>2</sub>H<sub>4</sub> (20 bar), at 250 °C for 1 h over various solid acid catalysts. Acid loading of all the oxide-supported HPAs = 15 wt%.

the highest PX product rate (77.98 mmol/(g.h)) with the highest PX selectivity (~70%).

HSiW/SiO<sub>2</sub> also exhibited higher PX production rate than H-BEA-25 (74.11 mmol/(g.h)), SAA-57 (54.97 mmol/(g.h)), and H-ZSM-5 (15.51 mmol/(g.h)), and higher selectivity to PX than those catalysts at similar DMF conversion (42–49%). In order to better compare the activity of different acid catalysts, the turnover frequency (TOF) for the production of PX over each catalyst was calculated, as shown in Table 1. Because Brønsted acidity determines the overall rate of PX production [16,18], the TOF was calculated by normalizing the rate of PX production by the number of proton sites. In the case of HPA/SiO<sub>2</sub>, the proton site densities were calculated assuming that all HPA protons (15 wt% loading) are equally available for the reaction. Similarly, for H-zeolites, the proton site densities were calculated from their Si/Al atomic ratios, assuming that the Al content is equal to the number of proton sites. It was found that the TOF values for HPW/SiO<sub>2</sub> (407.8 h<sup>-1</sup>) and HSiW/SiO<sub>2</sub> (371.3 h<sup>-1</sup>) were considerably greater than those for H-BEA-25 (60.0 h<sup>-1</sup>), HBEA-38 (72.8 h<sup>-1</sup>), and SAA-57 (47.4 h<sup>-1</sup>). The higher TOF values over HPA/SiO<sub>2</sub> suggest that they have stronger Brønsted acid sites, which can accelerate the rate of cycloadduct dehydration. Overall, silica-supported HPA catalysts demonstrated the superior activity and selectivity toward PX production than did zeolites and SAA.

**Table 2**

Summary of the catalytic performance results for DMF conversion to PX over various solid acid catalysts. Reaction condition: P = 20 bar, T = 250 °C, and t = 1 h.

Entry	Catalyst	X <sub>DMF</sub> (%)	S <sub>PX</sub> (%)	S <sub>HD</sub> (%)	S <sub>Oli</sub> (%)	C.B. (%)	PX rate (mmol/(g h))	TOF (h <sup>-1</sup> )
1	HPW*	41.22	50.52	0.00	1.38	82.11	169.21	7161.2
2	HPW	68.47	53.12	8.10	2.19	75.44	96.97	–
3	15%-HPW/SiO <sub>2</sub>	47.17	57.58	5.62	2.50	84.10	65.25	407.8
4	15%-HPW/Al <sub>2</sub> O <sub>3</sub>	9.65	17.25	0.00	4.89	92.49	3.90	24.4
5	15%-HPW/TiO <sub>2</sub>	5.24	8.03	0.00	0.00	95.18	1.21	6.90
6	15%-HPW/ZrO <sub>2</sub>	3.87	7.57	0.00	0.00	96.42	0.73	4.54
7	HSiW*	43.07	51.89	0.00	1.63	82.19	177.34	6626.4
8	HSiW	71.56	46.11	7.16	2.23	68.72	87.06	–
9	15%-HSiW/SiO <sub>2</sub>	42.36	69.81	4.95	0.29	89.60	77.98	371.3
10	15%-HSiW/Al <sub>2</sub> O <sub>3</sub>	44.62	50.14	3.54	3.83	81.36	55.01	266.3
11	15%-HSiW/TiO <sub>2</sub>	6.09	29.80	0.00	0.00	95.72	4.73	22.5
12	15%-HSiW/ZrO <sub>2</sub>	4.97	6.47	0.00	0.00	95.35	0.79	3.78
13	H-BEA-25	48.62	57.60	5.04	0.93	86.02	74.11	60.0
14	SAA-57	36.63	56.77	0.00	0.00	86.43	54.97	47.4
15	H-BEA-38	49.15	57.17	3.82	8.33	89.58	55.90	72.8
16	H-ZSM-5	10.77	69.15	0.00	0.00	96.68	15.51	16.1

Notation: \*m<sub>CAT</sub> = 0.05 g; X<sub>DMF</sub> = 2,5-dimethylfuran conversion, S<sub>PX</sub> = p-xylene selectivity, S<sub>HD</sub> = 2,5-heanedione selectivity, S<sub>Oli</sub> = oligomers selectivity; C.B. = carbon balance; TOF = turnover frequency, calculated as the p-xylene formation rate per surface proton site.

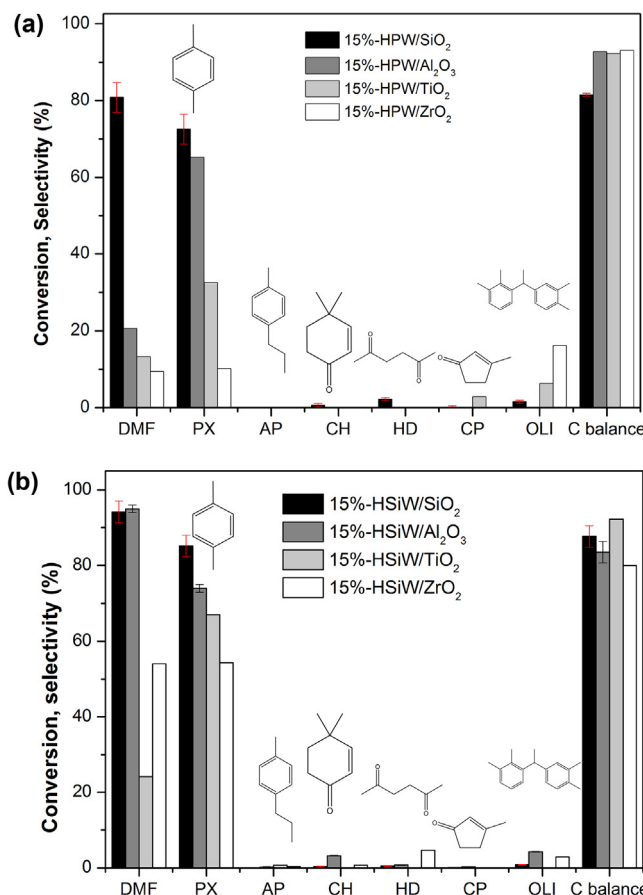


**Fig. 6.** DMF conversion, products selectivity, and carbon balance for the DA-reaction of DMF and C<sub>2</sub>H<sub>4</sub> (20–30 bar), at 250 °C for 6 h over oxide-supported HPW catalysts (a) and oxide-supported HSiW catalysts (b). Products are classified as p-xylene (PX), alkylated p-xylene (AP), 3,6-dimethyl-2-cyclohexenone (CH), 2,5-hexanedione (HD), 3-methyl-2-cyclopentenone (CP), and oligomers (OLI).

### 3.3. Effect of support on catalytic activity

The catalytic performances of all the oxide-supported HPAs were investigated further at an extended reaction time (6 h). Among all the different porous materials, silica appears to be the most effective catalyst support, either for the HPW or HSiW catalyst, and for both short (1 h) and extended reaction times. Fig. 6 clearly shows the superior performance of the silica-supported

HPAs and the PX selectivity decreases in the following order: HPA/SiO<sub>2</sub> > HPA/Al<sub>2</sub>O<sub>3</sub> > HPA/TiO<sub>2</sub> > HPA/ZrO<sub>2</sub>. In regard to the supported HPW, the highest PX selectivity (73%) was achieved over 15%-HPW/SiO<sub>2</sub> at approximately 81% DMF conversion. Regarding the supported HSiW, the highest PX selectivity (85%) was achieved over 15%-HSiW/SiO<sub>2</sub> at approximately 94% DMF conversion. The zirconia- and titania-supported HPAs consistently exhibited very low PX yields (<29%) at low DMF conversions (<54%).

The origin of the higher activity of the silica-supported HPAs for PX production was investigated. According to the literature, the overall rate of PX formation has a linear dependence on the density of Brønsted acid sites in the catalysts [19]. This is because the initial DA reaction of DMF and ethylene is a thermal process, while the dehydration of the DMF/ethylene cycloadduct cannot proceed uncatalyzed, thereby making the second dehydration the rate-limiting step for PX production [15]. Therefore, the correlation between the acid site density estimated from TPD of ammonia and the initial rate of PX production was examined. The acid site density of the supported HPA catalysts was modified by subtracting the support acidity from the overall acidity of the supported HPA catalysts in order to consider only the Brønsted acid sites. Because impregnated HPW and HSiW species contain predominantly Brønsted acid sites, the calculated acidity can be a reasonable approximation of the density of Brønsted acid sites. As shown in Fig. 7(a), the PX production rate was proportional to the acid site concentration with bulk HSiW, which possesses the highest acid concentration (2.30 mmol/g), with the highest rate of PX production (177.34 mmol/(g h)). The silica-supported HPAs, which possess the higher acid site concentrations, exhibited the higher PX production rates than other oxide-supported HPAs. These results suggest that the high activity of the silica-supported HPAs is mainly due to their high concentration of Brønsted acid sites.

In addition to the acid site concentrations, the acid strength can affect the catalytic activity. It has been reported that an interaction between HPA and the oxide supports can largely influence the acid strength of the HPA catalysts. According to the initial enthalpies of ammonia adsorption ( $\Delta H_{NH_3}$ ) for the HPA catalysts measured by NH<sub>3</sub> adsorption calorimetry, the acid strength of the HPA catalysts decreased in the order: HPW > HSiW > HPW/SiO<sub>2</sub> ≈ HSiW/SiO<sub>2</sub> > HPW/TiO<sub>2</sub> > HPW/ZrO<sub>2</sub> [24,30,39]. The supported HPA catalysts exhibited the weaker acidity than the bulk HPAs owing to the interaction of HPAs with the supports, and the acid strength of the supported HPA catalysts decreased with increasing HPA-support interaction. Although the NH<sub>3</sub> adsorption calorimetry technique does not discriminate Brønsted and Lewis acid sites, the measured acid strength showed

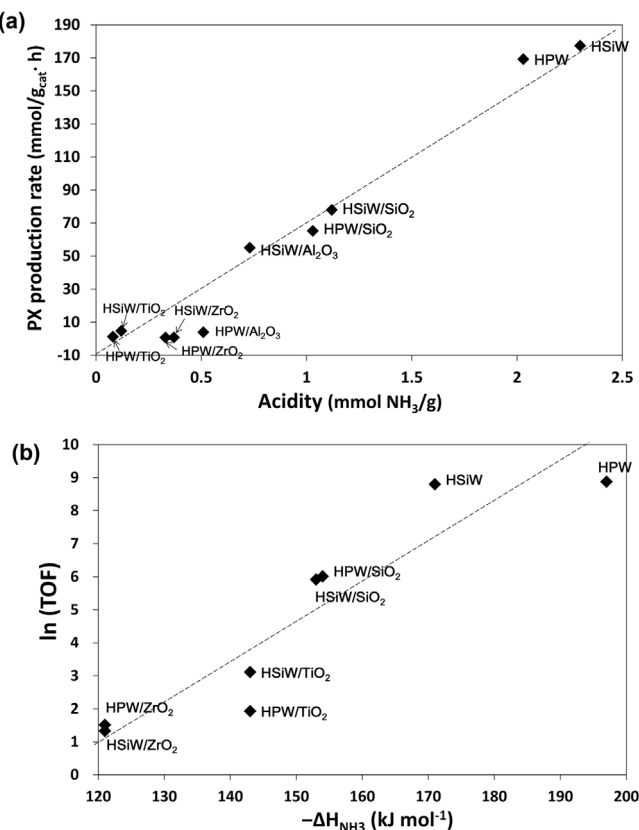


**Fig. 7.** Correlations (a) between surface acidity and PX production rate and (b) between initial heat of NH<sub>3</sub> adsorption and TOF.

a good correlation with the rate of acid-catalyzed reaction (e.g., methanol dehydration) [30]. Accordingly, the correlation between the acid strength and the turnover frequency (TOF) of PX formation was examined, as shown in Fig. 7(b). TOFs for the supported HPA catalysts were calculated per surface Brønsted site, assuming that all HPA protons were equally available for the reaction. On the other hand, in the case of bulk HPAs, the proton site densities were calculated using a Keggin unit cross section of 144 Å<sup>2</sup> and the catalyst surface areas (i.e., HPW = 0.023 mmol (H<sup>+</sup>) g<sup>-1</sup> and HSiW = 0.023 mmol (H<sup>+</sup>) g<sup>-1</sup>) to consider only surface proton site. Notably, a linear relationship was observed between the TOF and catalyst acid strength, showing that the higher the acid strength, the higher the turnover rate of PX formation. Therefore, this result suggests that the higher activity of HPA/SiO<sub>2</sub> for PX production is at least partly due to the enhanced strength of Brønsted acid sites.

#### 3.4. Effect of the reaction conditions

As the best-performing catalyst in this study, the silica-supported HSiW was used to investigate further the effect of reaction conditions, such as acid loading, reaction temperature, and reaction time on the DMF conversion and PX selectivity. As shown in Fig. 8, increasing the HSiW loading from 5 to 15 wt% resulted in increasing DMF conversion, PX selectivity, and PX yield, as expected. However, when the acid loading was increased further to 20 wt%, the DMF conversion and PX selectivity decreased slightly. This probably indicates that 15 wt% is the optimal acid loading for submonolayer coverage in the HSiW/SiO<sub>2</sub>, in which all the HPA protons are equally available for the reaction.

The reaction temperature, as shown in Fig. 9, also affects the conversion of DMF to PX. Over the HSiW supported on silica, DMF conversion increases linearly from 35 to 91% and the PX selectivity

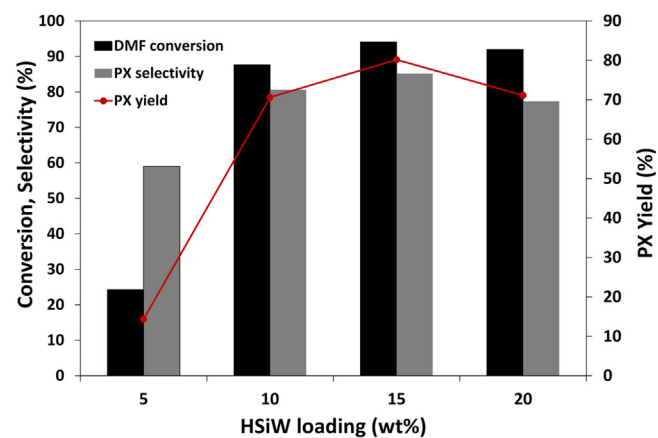


**Fig. 8.** DMF conversion, PX selectivity and yield for the DA-reaction of DMF and C<sub>2</sub>H<sub>4</sub> (30 bar) at 250 °C for 6 h in over HSiW/SiO<sub>2</sub> with different acid loadings (5–20 wt%).

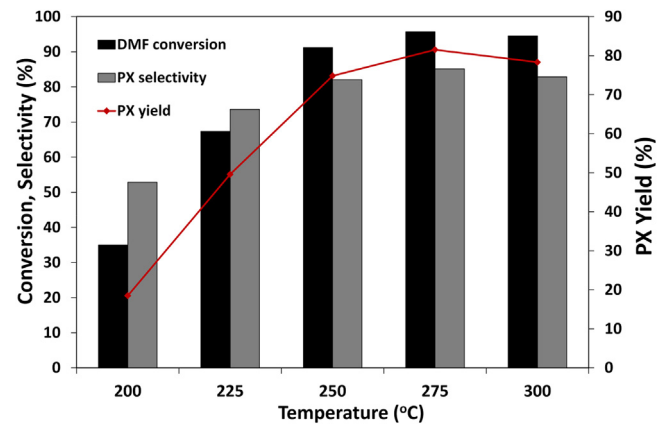


**Fig. 9.** DMF conversion, PX selectivity and yield for the DA-reaction of DMF and C<sub>2</sub>H<sub>4</sub> (30 bar) at different temperatures (200–300 °C) for 6 h over 15%-HSiW/SiO<sub>2</sub>.

also increases sharply from 53 to 82% with increasing temperature from 200 to 250 °C. Interestingly, when the reaction temperature was increased further to 275 °C, the DMF conversion and PX selectivity also increased slightly to 96 and 85%, respectively. Even at 300 °C, the DMF conversion and PX selectivity were still high (95 and 83%, respectively), indicating that the 15%-HSiW/SiO<sub>2</sub> has good thermal stability in the reaction and it is not easily deactivated by coke under high temperature reaction conditions (>250 °C). As summarized in Table S4, the carbon balances for all the reactions at different temperatures are relatively constant (84–86%), suggesting that the higher reaction temperature does not necessarily promote the formation of larger oligomers or solid residues.

In addition to the acid loading and reaction temperature, the effects of the reaction time were also investigated over 15%-HSiW/SiO<sub>2</sub> in comparison to the commercial zeolite, H-BEA-25. Fig. 10 clearly shows that both catalysts show similar DMF conversion profiles. However, the PX production rates over 15%-HSiW/SiO<sub>2</sub> were higher than those over H-BEA-25. The highest PX yield over 15%-HSiW/SiO<sub>2</sub> was 82% within 8 h, whereas over H-BEA-25, it took longer time (12 h) for a lower PX yield (68%). Importantly, as mentioned previously in the effects of the reaction temperature, the carbon balances for the different reaction times with 15%-HSiW/SiO<sub>2</sub> were also relatively constant (84–88%), and no apparent change was observed. Meanwhile, at a longer reaction time, the carbon balance for the reaction with H-BEA-25 was much lower (77%) due to the more significant formation of byproducts (such as alkylated products and oligomers) and the possible formation of a solid residue (coke) on the catalyst, as confirmed by the

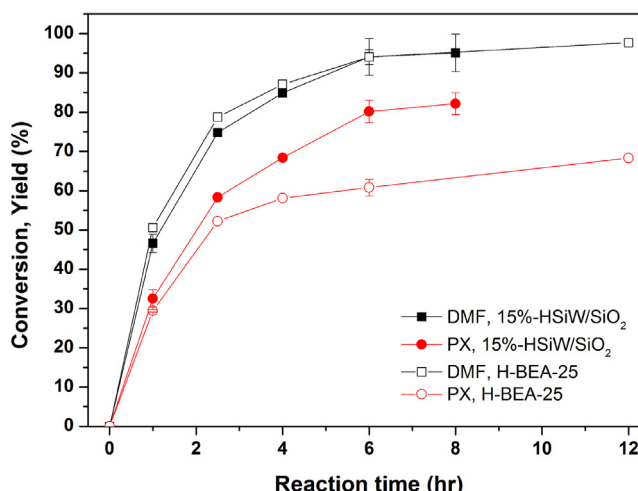


**Fig. 10.** DMF conversion and PX yield as a function of time for the DA-reaction of DMF and C<sub>2</sub>H<sub>4</sub> (30 bar) at 250 °C over 15%-HSiW/SiO<sub>2</sub> in comparison to H-BEA-25.

**Table 3**

Summary of the catalytic performance results for DMF conversion to PX over the fresh and spent HSiW/SiO<sub>2</sub> catalysts calcined at different temperatures. Reaction condition: P = 30 bar and T = 250 °C.

Catalyst	t (h)	X <sub>DMF</sub> (%)	Y <sub>PX</sub> (%)	S <sub>PX</sub> (%)	C.B. (%)
Fresh, calcined at 100 °C	6	94.1	80.2	85.2	87.7
Spent, uncalcined	6	65.1	49.4	76.0	85.4
Spent, calcined at 325 °C	6	10.1	3.1	30.7	93.0
Spent, calcined at 400 °C	6	51.7	37.8	73.1	86.2
Spent, calcined at 550 °C	6	1.6	0.5	33.2	98.9
Fresh, calcined at 100 °C	1	46.2	29.1	63.0	81.1
Fresh, calcined at 300 °C	1	50.6	29.8	58.9	78.0
Fresh, calcined at 400 °C	1	26.5	10.2	38.6	76.8
Fresh, calcined at 500 °C	1	0.3	-	-	-

GC/MS spectra for the liquid products from the reactions shown in Figs. S6 and S7.

### 3.5. Reusability of HSiW/SiO<sub>2</sub> catalysts

The stability and reusability of HSiW/SiO<sub>2</sub> catalysts were investigated. For this purpose, the spent catalyst from the reaction of DMF and ethylene was reused under the standard reaction conditions. As shown in Table 3, the recycled catalyst showed a lower DMF conversion than the fresh HSiW/SiO<sub>2</sub> (65.1% vs 94.1%) and a lower selectivity to PX (76% vs 85.2%). Thermogravimetric (TG) analysis of the spent catalyst revealed the formation of carbonaceous deposits on the spent catalyst, comprising of approximately 5% of the catalyst weight (see Fig. 11). In the meantime, Inductively Coupled Plasma (ICP-OES) analysis of the product solution indicated that HSiW (tungsten species) leaching is negligible (<1%). Therefore, the deactivation of the HSiW/SiO<sub>2</sub> can be attributed to the loss of some active sites by deposition of coke.

Because the DTG curve of the spent catalyst showed a peak at 450 °C, the calcination temperature of the spent catalyst for regeneration was explored at a temperature ranging from 325 to 550 °C. The catalysis results showed that 400 °C was the optimal temperature for calcination, but the initial activity of the catalyst could not be fully regained, showing only 51.7% conversion and 73.1% PX selectivity. TGA analyses of the spent catalysts calcined at different temperatures confirmed that the calcination temperature above 400 °C is required to fully remove the coke. The XRD measurements showed that the calcination temperature of 550 °C results in the decomposition of Keggin structure, forming WO<sub>3</sub> crystallites, while the Keggin structure is intact at the calcination temperatures below

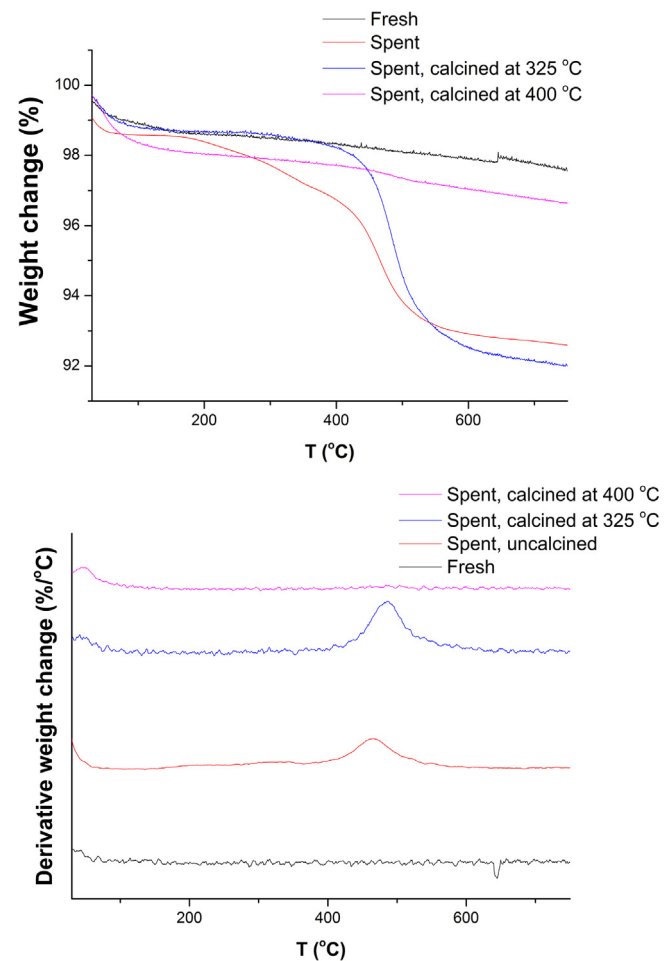


**Fig. 11.** TGA and DTG curves for the fresh and spent HSiW/SiO<sub>2</sub> catalysts.

400 °C (see Fig. S7). Overall, TGA and XRD measurements suggest that the coke can be completely removed after calcination at 400 °C without the decomposition of Keggin structure, but the catalyst activity was not fully recovered. In order to clarify the reason behind the lower activity of the spent catalyst calcined at 400 °C, the fresh catalyst was also subjected to calcination at different temperatures and was tested for the reaction. The activity was found to be much dependent on the calcination temperature. The activity of the catalyst was highest in the calcination temperature of 100 and 300 °C, showing the DMF conversion of 45 and 50% at 1 h reaction time and was decreased by half (26.5% DMF conversion) with an increase in the calcination temperature to 400 °C. This result implies that the calcination should be carried out at temperatures below 300 °C for the regeneration of the spent catalyst to keep the highest activity of HSiW/SiO<sub>2</sub> catalyst; however, the coke could not be removed at such low temperatures as seen in the TGA results. The decrease in the activity of the catalyst calcined at 400 °C might be due to the partial degradation of Keggin structure of HSiW supported on silica, affecting its acidity. Thus, the challenge remains to establish the method for regenerating the coked HSiW/SiO<sub>2</sub> catalyst.

### 4. Conclusions

In summary, silica-supported HSiW demonstrated remarkable catalytic performance for PX production from DMF (~82% yield) and should be considered as a promising catalyst for this reaction among all the oxide-supported HPA catalysts. Importantly, the turnover frequency of PX production for

HSiW/SiO<sub>2</sub> was 6–8 times greater than those for HBEA-25 and SAA-57, which were previously reported as highly active catalysts. Compared to other oxide-supported HPAs, the higher activity of HPA/SiO<sub>2</sub> was mainly due to their higher acid site density and stronger Brønsted acidity. Results from NH<sub>3</sub>-TPD showed that the total acidity of the catalysts decreased in the order HPA/SiO<sub>2</sub>>HPA/Al<sub>2</sub>O<sub>3</sub>>HPA/ZrO<sub>2</sub>>HPA/TiO<sub>2</sub>, while the rate of PX production decreased in the order HPA/SiO<sub>2</sub>>HPA/Al<sub>2</sub>O<sub>3</sub>>HPA/TiO<sub>2</sub>>HPA/ZrO<sub>2</sub>. The turnover frequency of PX production for bulk and silica-supported HPA catalysts were also significantly greater than those for HPAs supported on TiO<sub>2</sub> and ZrO<sub>2</sub>, indicating that the weak interaction of silica with the HPAs allow them to keep strong Brønsted acidity, thereby accelerating the rate of cycloadduct dehydration. Both the silica-supported HSiW and HPW catalysts were capable of producing remarkably high PX selectivity (82–85%) at high DMF conversion (91–94%) at 250 °C after 6 h reaction. Overall, the silica-supported HPAs can be an alternative potential catalyst for the tandem DA and dehydration reactions of DMF and ethylene to produce PX with high selectivity. This study would contribute to the design and development of improved catalysts for the efficient synthesis of renewable chemicals from biomass, as a part of the sustainable efforts to reduce the dependency on petroleum-derived chemicals.

## Acknowledgements

This research was supported by the National Research Council of Science & Technology (NST) grant by the Korea government (MSIP) (No. CAP-11-04-KIST). This work was also supported by the New & Renewable Energy Core Technology Program of the Korea Institute of Energy Technology Evaluation and Planning (KETEP) granted financial resource from the Ministry of Trade, Industry & Energy, Republic of Korea (No. 20153030101580).

## Appendix A. Supplementary data

Supplementary data associated with this article can be found, in the online version, at <http://dx.doi.org/10.1016/j.cattod.2016.12.032>.

## References

- [1] T.R. Carlson, Y.-T. Cheng, J. Jae, G.W. Huber, *Energy Environ. Sci.* 4 (2011) 145–161.
- [2] T.R. Carlson, G.A. Tompsett, W.C. Conner, G.W. Huber, *Top. Catal.* 52 (2009) 241–252.

- [3] S.K. Green, R.E. Patet, N. Nikbin, C.L. Williams, C.-C. Chang, J. Yu, R.J. Gorte, S. Caratzoulas, W. Fan, D.G. Vlachos, *Appl. Catal. B* 180 (2016) 487–496.
- [4] D.I. Collias, A.M. Harris, V. Nagpal, I.W. Cottrell, M.W. Schultheis, *Ind. Biotechnol.* 10 (2014) 91–105.
- [5] J.J. Pacheco, M.E. Davis, *Proc. Natl. Acad. Sci. U. S. A.* (2014) 201408345.
- [6] Y. Tachibana, S. Kimura, K.-i. Kasuya, *Sci. Rep.* 5 (2015).
- [7] A. Illanes, M. Zuniga, S. Contreras, A. Guerrero, *Bioprocess. Eng.* 7 (1992) 199–204.
- [8] M. Moliner, Y. Román-Leshkov, M.E. Davis, *Proc. Natl. Acad. Sci. U. S. A.* 107 (2010) 6164–6168.
- [9] Y. Román-Leshkov, C.J. Barrett, Z.Y. Liu, J.A. Dumesic, *Nature* 447 (2007) 982–985.
- [10] J. Jae, W. Zheng, R.F. Lobo, D.G. Vlachos, *ChemSusChem* 6 (2013) 1158–1162.
- [11] Y. Lin, S. Tanaka, *Appl. Microbiol. Biotechnol.* 69 (2006) 627–642.
- [12] A. Morschbacker, J. Macromol. Sci. Polym. Rev. 49 (2009) 79–84.
- [13] M. Zhang, Y. Yu, *Ind. Eng. Chem. Res.* 52 (2013) 9505–9514.
- [14] C.L. Williams, C.-C. Chang, P. Do, N. Nikbin, S. Caratzoulas, D.G. Vlachos, R.F. Lobo, W. Fan, P.J. Dauenhauer, *ACS Catal.* 2 (2012) 935–939.
- [15] N. Nikbin, P.T. Do, S. Caratzoulas, R.F. Lobo, P.J. Dauenhauer, D.G. Vlachos, *J. Catal.* 297 (2013) 35–43.
- [16] D. Wang, C.M. Osmundsen, E. Taarning, J.A. Dumesic, *ChemCatChem* 5 (2013) 2044–2050.
- [17] C.-C. Chang, S.K. Green, C.L. Williams, P.J. Dauenhauer, W. Fan, *Green Chem.* 16 (2014) 585–588.
- [18] Y.P. Wijaya, D.J. Suh, J. Jae, *Catal. Commun.* 70 (2015) 12–16.
- [19] R.E. Patet, N. Nikbin, C.L. Williams, S.K. Green, C.-C. Chang, W. Fan, S. Caratzoulas, P.J. Dauenhauer, D.G. Vlachos, *ACS Catal.* 5 (2015) 2367–2375.
- [20] T.-W. Kim, S.-Y. Kim, J.-C. Kim, Y. Kim, R. Ryoo, C.-U. Kim, *Appl. Catal. B* 185 (2016) 100–109.
- [21] S. Song, G. Wu, W. Dai, N. Guan, L. Li, *J. Mol. Catal. A: Chem.* 420 (2016) 134–141.
- [22] I.V. Kozhevnikov, *Chem. Rev.* 98 (1998) 171–198.
- [23] Y. Izumi, R. Hasebe, K. Urabe, *J. Catal.* 84 (1983) 402–409.
- [24] A.M. Alsalme, P.V. Wiper, Y.Z. Khimyak, E.F. Kozhevnikova, I.V. Kozhevnikov, *J. Catal.* 276 (2010) 181–189.
- [25] J.K. Kim, J.H. Choi, J.H. Song, J. Yi, I.K. Song, *Catal. Commun.* 27 (2012) 5–8.
- [26] M. Mizuno, N. Mizuno, K. Katamura, A. Kasai, Y. Konishi, K. Sakata, T. Okuhara, Y. Yoneda, *Bull. Chem. Soc. Jpn.* 55 (1982) 400–406.
- [27] N. Mizuno, M. Mizuno, *Curr. Opin. Solid State Mater. Sci.* 2 (1997) 84–89.
- [28] I. Kozhevnikov, K. Kloetstra, A. Sinnema, H. Zandbergen, H. Van Bekkum, *J. Mol. Catal. A: Chem.* 114 (1996) 287–298.
- [29] R.M. Ladera, J.L.G. Fierro, M. Ojeda, S. Rojas, *J. Catal.* 312 (2014) 195–203.
- [30] W. Alharbi, E.F. Kozhevnikova, I.V. Kozhevnikov, *ACS Catal.* 5 (2015) 7186–7193.
- [31] B.B. Bardin, R.J. Davis, *Appl. Catal.* 200 (2000) 219–231.
- [32] M. Timofeeva, *Appl. Catal. A* 256 (2003) 19–35.
- [33] J.C. Juan, J. Zhang, M.A. Yarmo, *J. Mol. Catal. A: Chem.* 267 (2007) 265–271.
- [34] A.H. Jadhav, H. Kim, I.T. Hwang, *Bioresour. Technol.* 132 (2013) 342–350.
- [35] H. Atia, U. Armbruster, A. Martin, *J. Catal.* 258 (2008) 71–82.
- [36] S.M. Kumbar, G. Shanbhag, F. Lefebvre, S. Halligudi, *J. Mol. Catal. A: Chem.* 256 (2006) 324–334.
- [37] T.H. Kang, J.H. Choi, Y. Bang, J. Yoo, J.H. Song, W. Joe, J.S. Choi, I.K. Song, *J. Mol. Catal. A: Chem.* 396 (2015) 282–289.
- [38] C. Pereira, R. Gorte, *Appl. Catal. A* 90 (1992) 145–157.
- [39] W. Alharbi, E. Brown, E.F. Kozhevnikova, I.V. Kozhevnikov, *J. Catal.* 319 (2014) 174–181.